

Supplementary information: Skyrmionium – Semicircular Magnetic Defect Interaction on a Racetrack

S. Navarro-Vilca¹, S. Urcia-Romero², and H. Vigo-Cotrina³

¹Departamento de Física Aplicada, Universidad Nacional Jorge Basadre Grohmann,
Avenida Miraflores, S/N, Ciudad Universitaria, Tacna 23003, Perú

²Department of Physics, University of Puerto Rico,
Mayagüez, Puerto Rico 00681, USA

³Grupo de Investigación en Ciencias Aplicadas y Nuevas Tecnologías, Universidad
Privada del Norte,
Trujillo, Perú

Corresponding author: helmunt.vigo@upn.edu.pe

1) Skyrmionium–Magnetic Defect Interaction Energy

Interaction energies were obtained using equation (1) as given in the main article. Each term of the equation was obtained using the MuMax [1] built-in function `relax()`, which calculates the system ground state. The origin of the coordinates is located in the center of the racetrack.

1.1) Skyrmionium–Semicircular Magnetic Defect Interaction Energy with a width of $W = 512$ nm

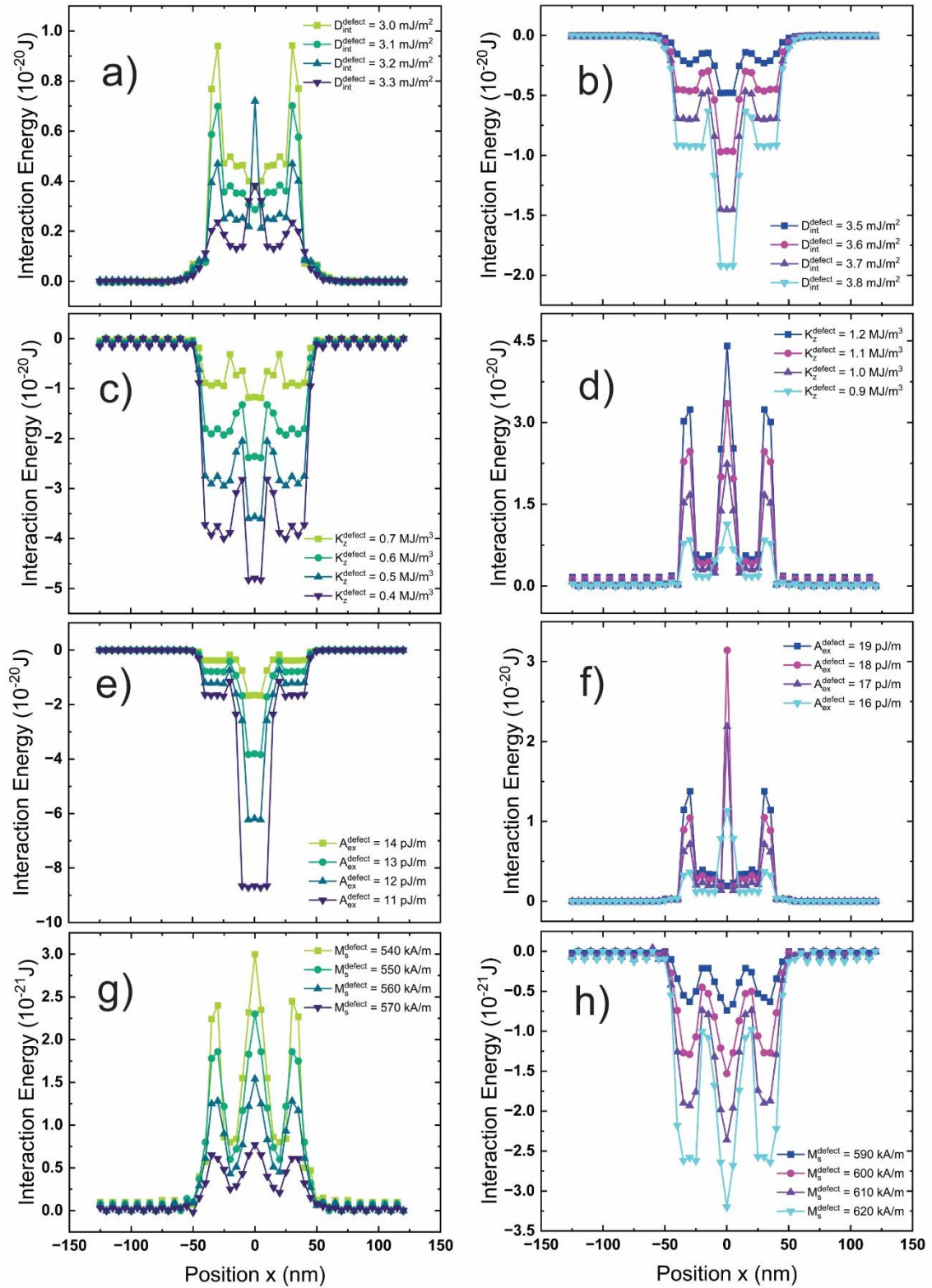


Fig. S1. Interaction energy between the skyrmionium and the defect ($\rho = 20$ nm) obtained by micromagnetic simulation using eq. (1) considering different defect parameters with a width of $W = 512$ nm.

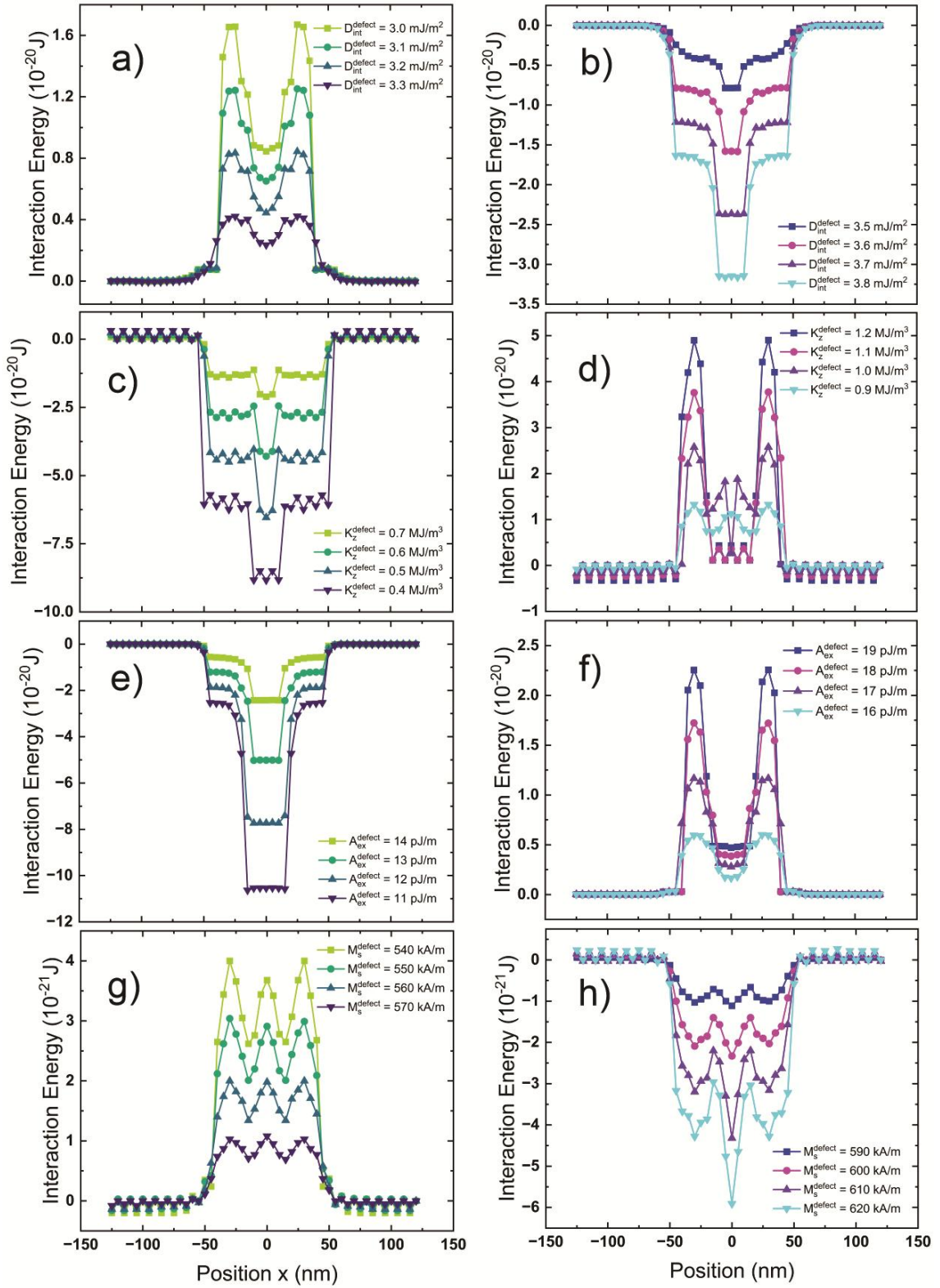


Fig. S2. Interaction energy between the skyrmionium and the defect ($\rho = 30$ nm) obtained by micromagnetic simulation using eq. (1) considering different defect parameters with a width of $W = 512$ nm.

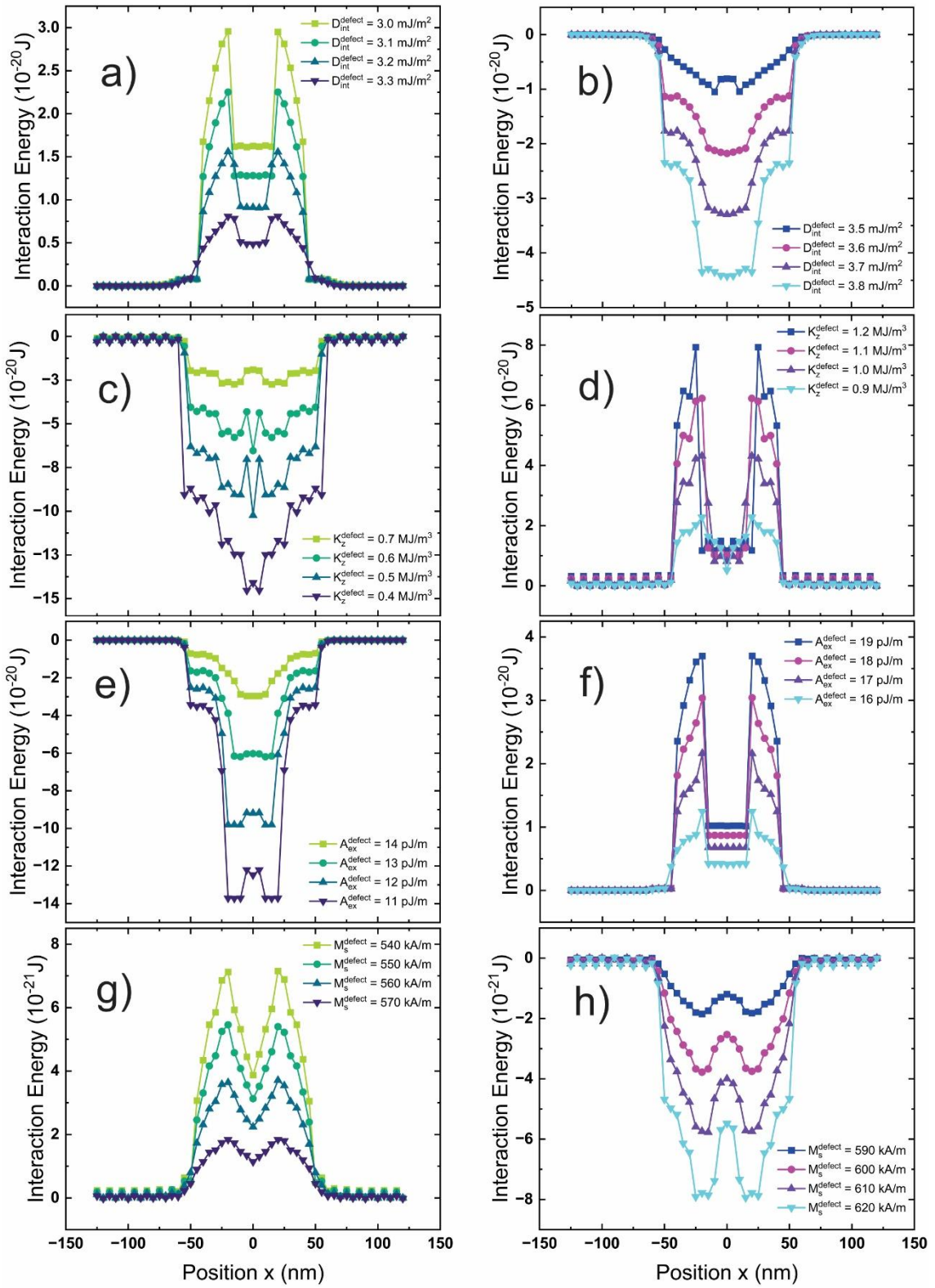


Fig. S3. Interaction energy between the skyrmionium and the defect ($\rho = 40$ nm) obtained by micromagnetic simulation using eq. (1), considering different defect parameters with a width of $W = 512$ nm.

1.2) Skyrmionium–Semicircular Magnetic Defect Interaction Energy with a width of $W = 256$ nm.

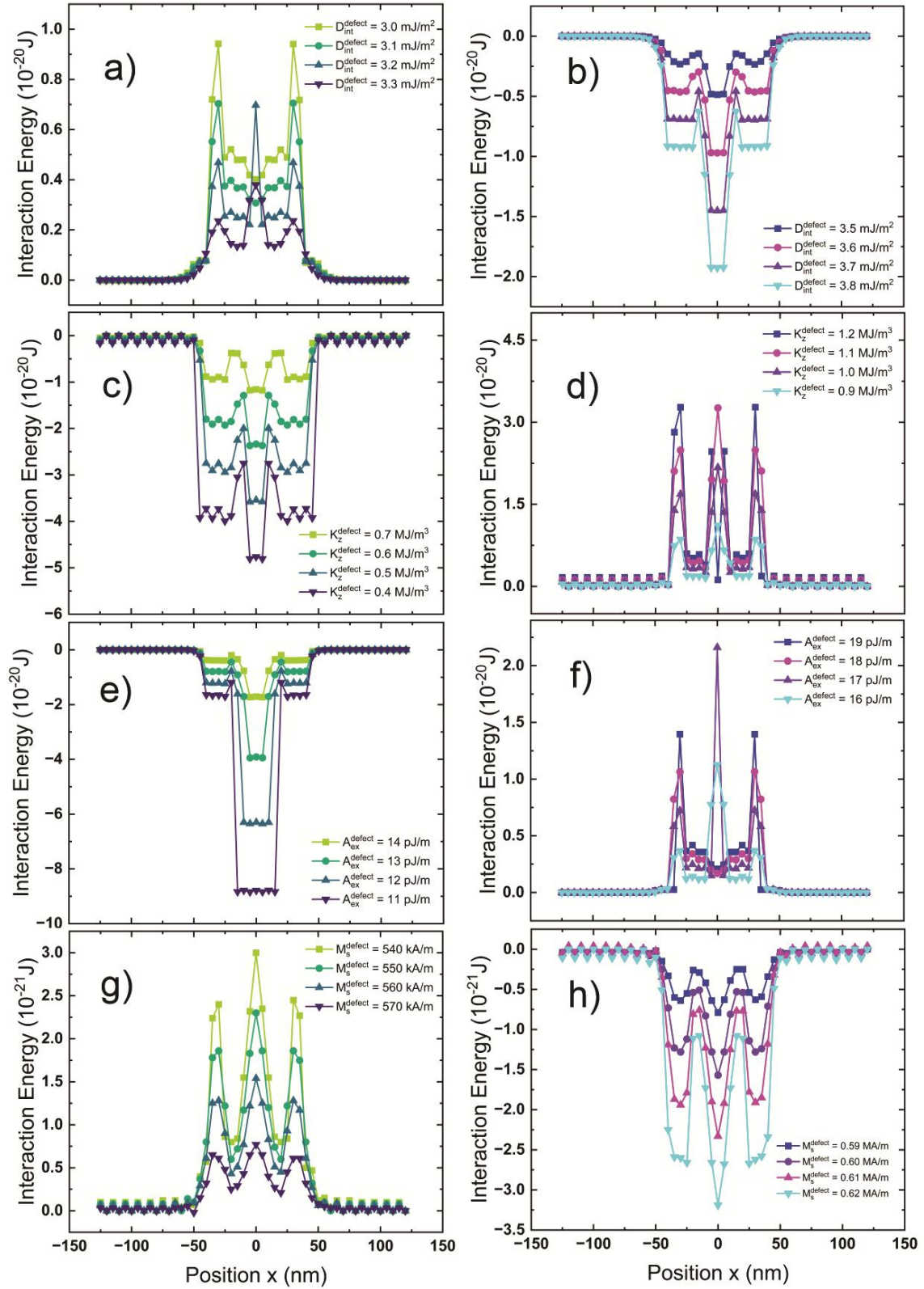


Fig. S4. Interaction energy between the skyrmionium and the defect ($\rho = 20$ nm) obtained by

micromagnetic simulation using eq. (1) considering different defect parameters with a width of $W = 256$ nm.

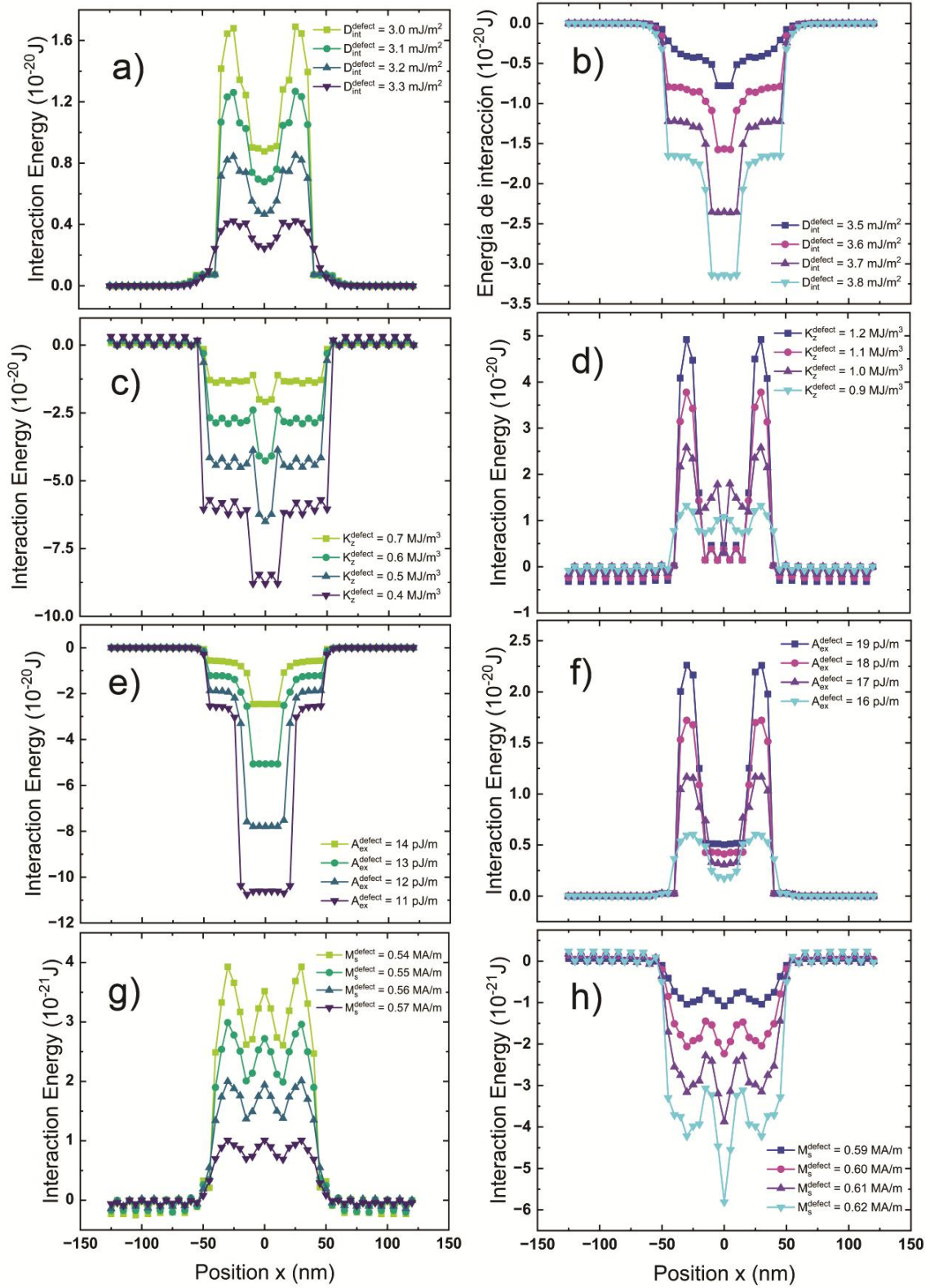


Fig. S5. Interaction energy between the skyrmionium and the defect ($\rho = 30$ nm) obtained by micromagnetic simulation using eq. (1) considering different defect parameters with a width of $W = 256$ nm.

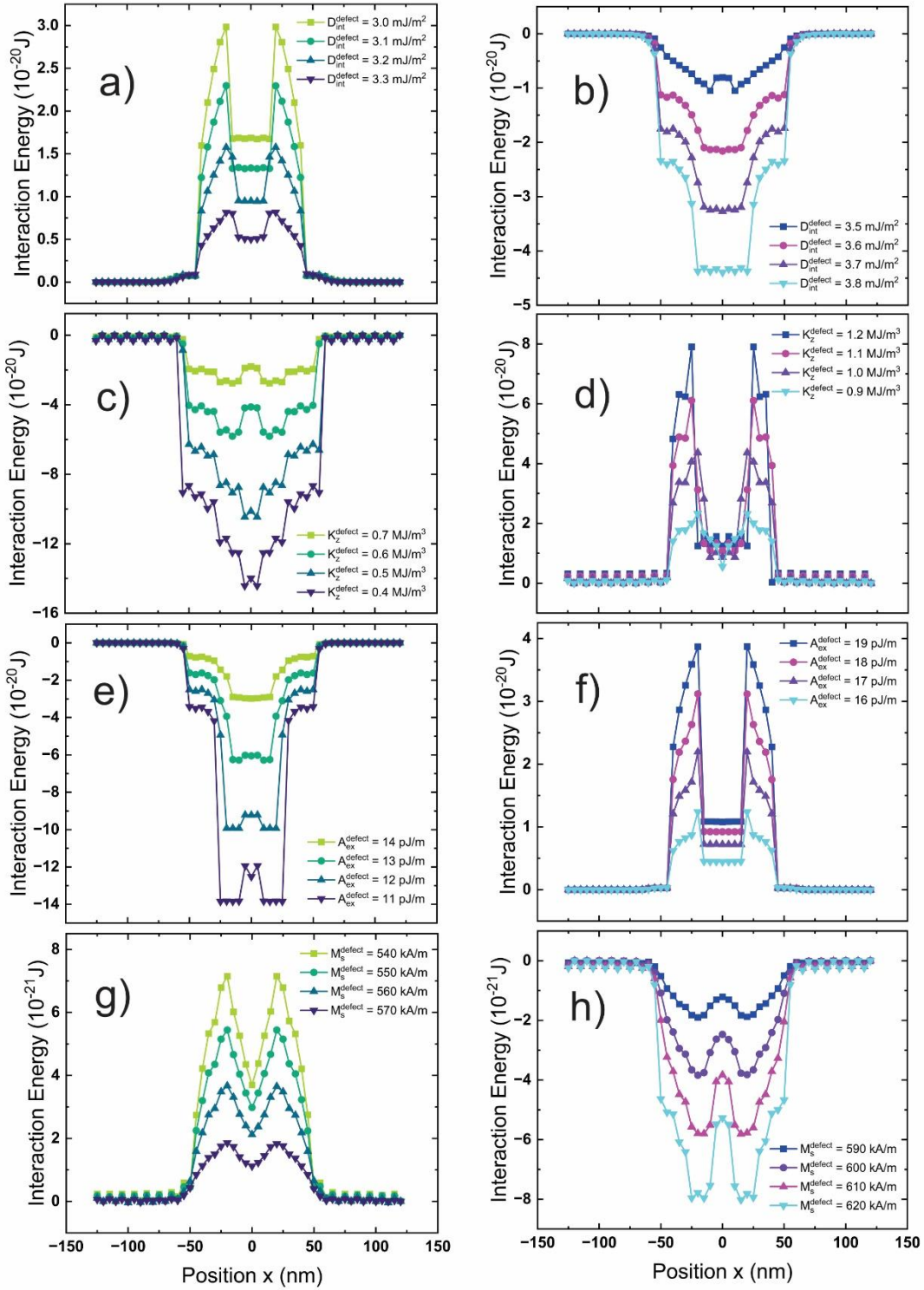


Fig. S6. Interaction energy between the skyrmionium and the defect ($\rho = 40$ nm) obtained by micromagnetic simulation using eq. (1) considering different defect parameters with a width of $W = 256$ nm.

1.3) Skyrmionium–Semicircular Magnetic Defect Interaction Energy with a width of $W = 128$ nm.

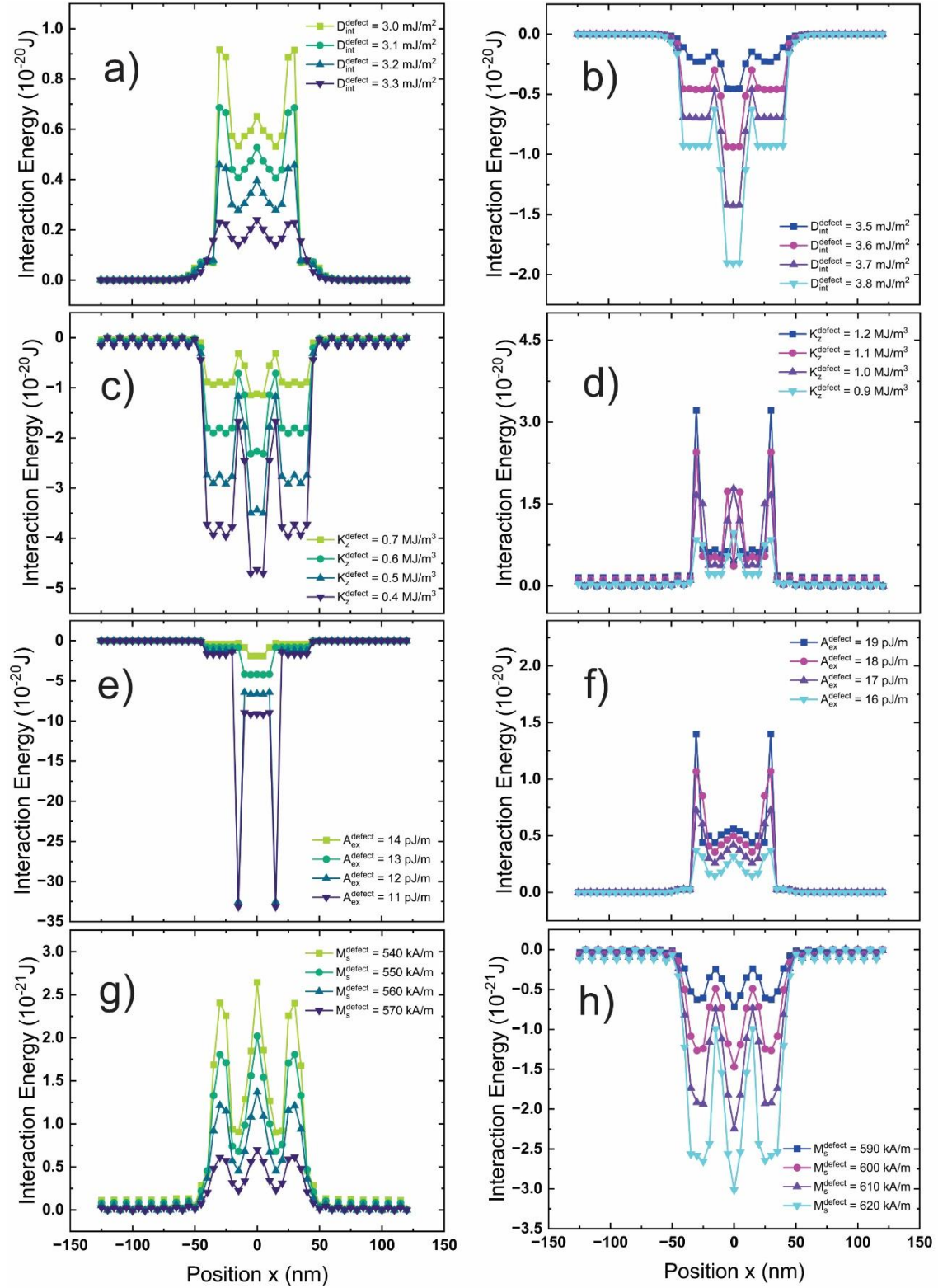


Fig. S7. Interaction energy between the skyrmionium and the defect ($\rho = 20$ nm) obtained by

micromagnetic simulation using eq. (1) considering different defect parameters with a width of $W = 128$ nm.

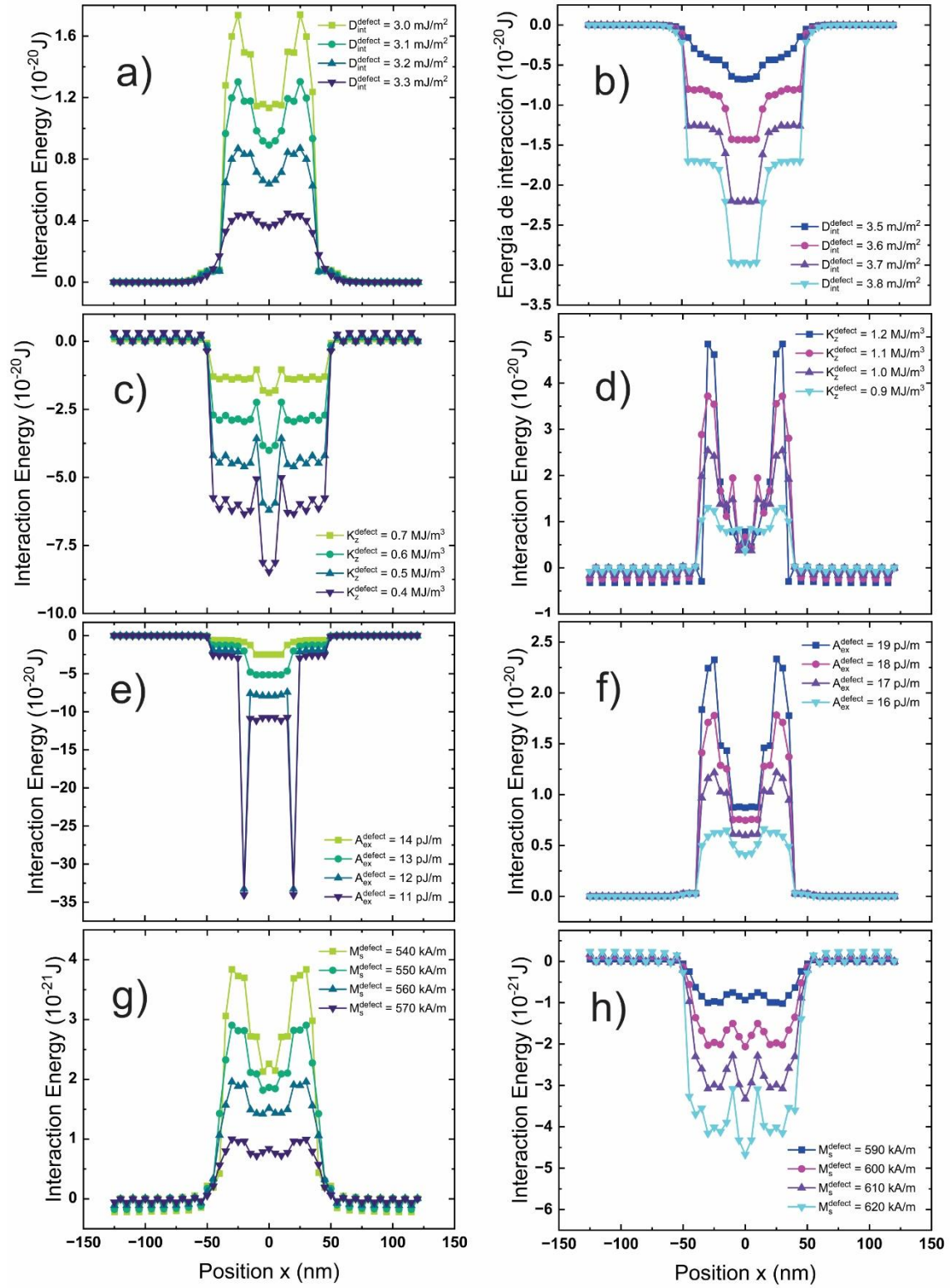


Fig. S8. Interaction energy between the skyrmionium and the defect ($\rho = 30$ nm) obtained by micromagnetic simulation using eq. (1) considering different defect parameters with a width of $W = 128$ nm.

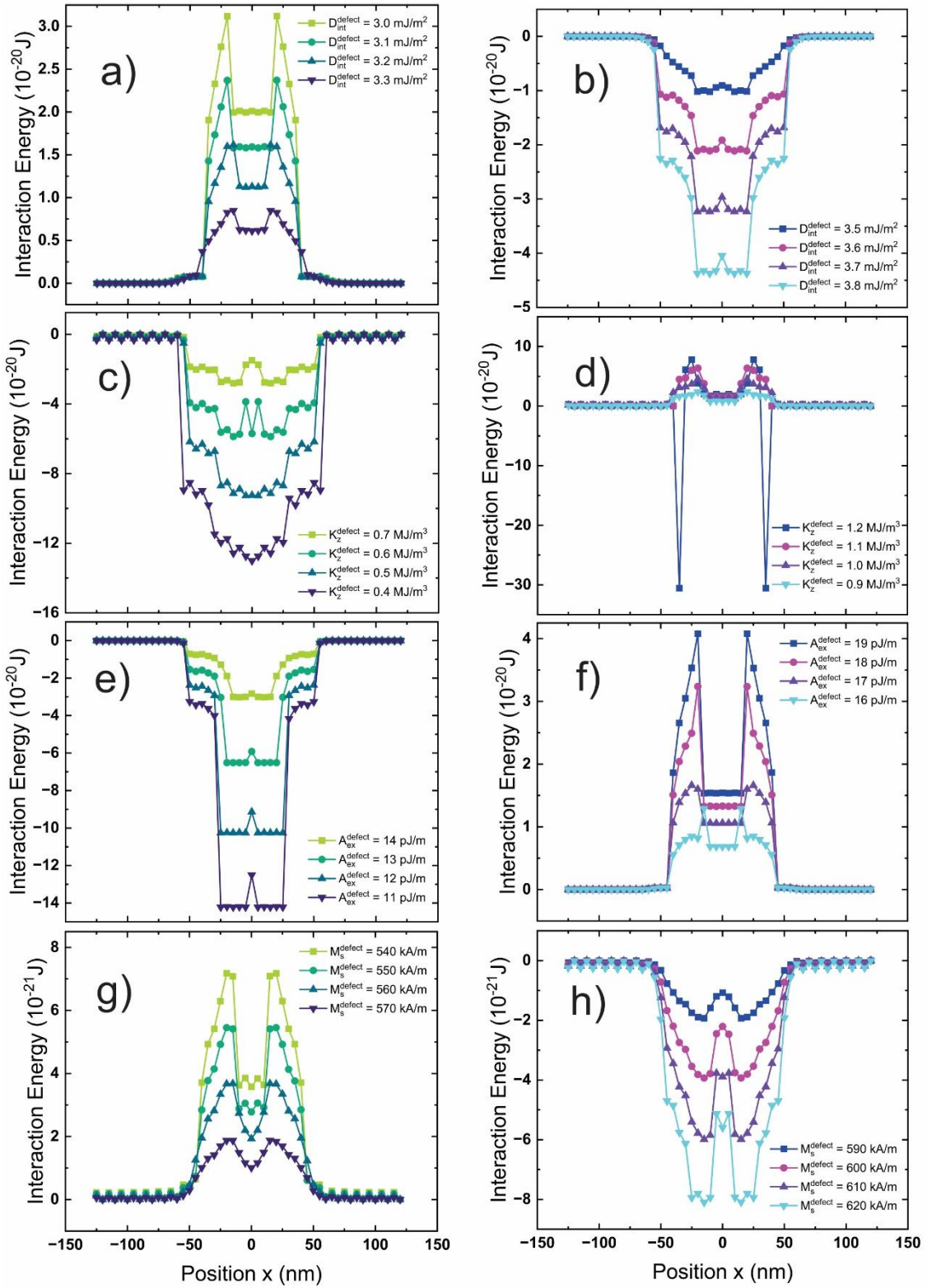


Fig. S9. Interaction energy between the skyrmionium and the defect ($\rho = 40$ nm) obtained by micromagnetic simulation using eq. (1) considering different defect parameters with a width of $W = 128$ nm.

2) Phase diagrams for different values for the width W .

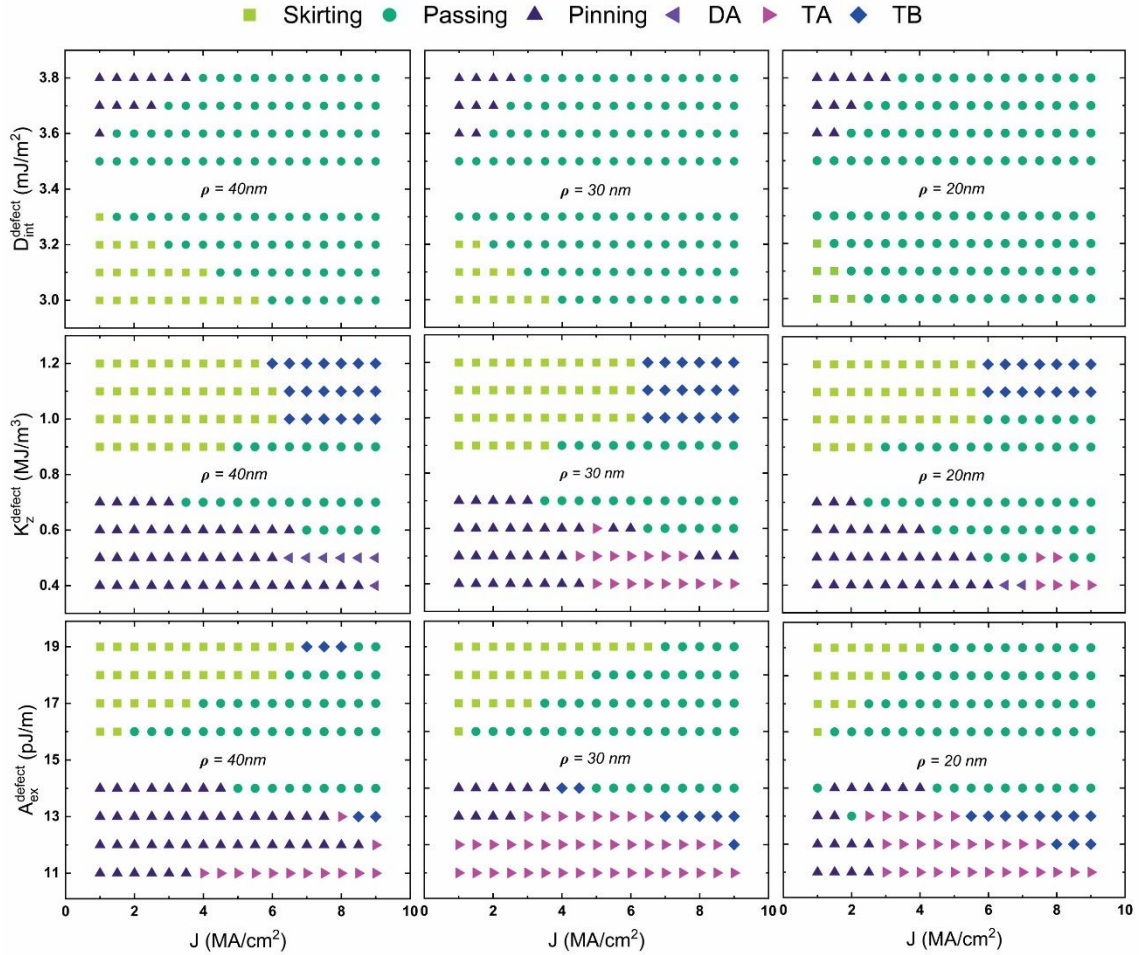


Fig. S10. The phase diagrams of possible states for the skyrmionium dynamics in the presence of a magnetic defect depict a wide range of physical parameters and diameters, offering a comprehensive view of the system's behavior for a width $W = 128 \text{ nm}$.

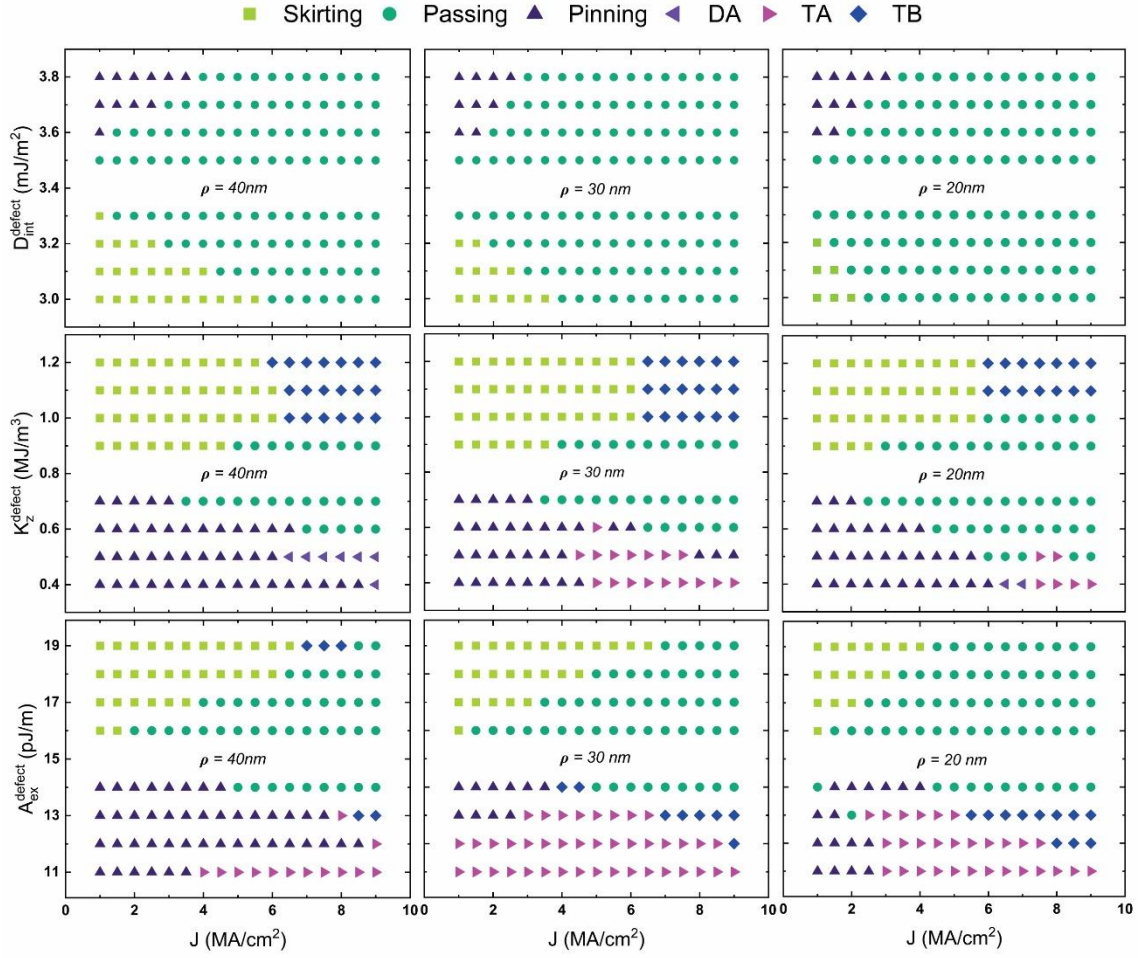


Fig. S11. The phase diagrams of possible states for the skyrmionium dynamics in the presence of a magnetic defect depict a wide range of physical parameters and diameters, offering a comprehensive view of the system's behavior for a width $W = 256$ nm.

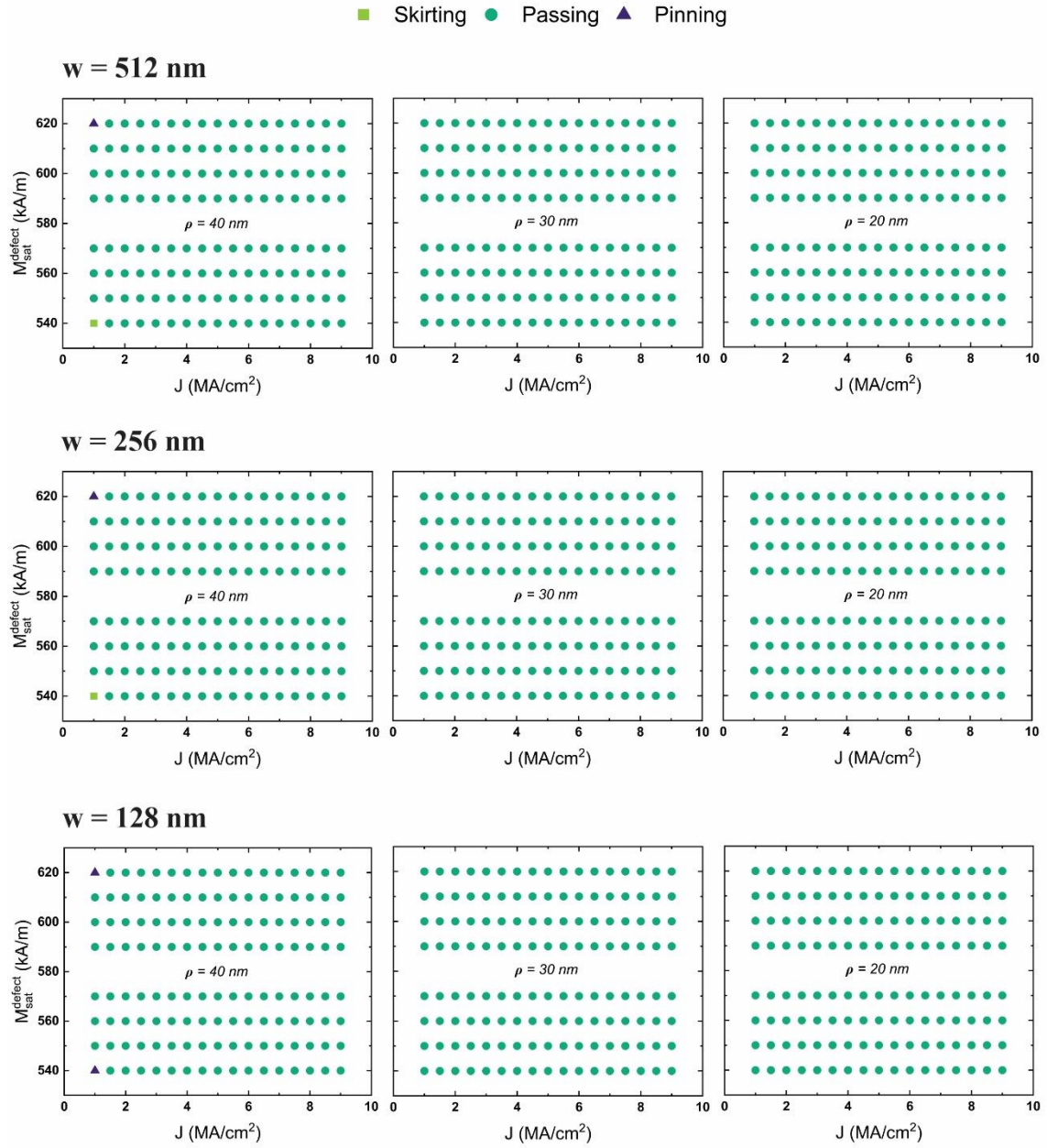


Fig. S12. Phase diagrams showing all possible skyrmionium dynamics states in the presence of a defect, with its saturation magnetization value M_{sat}^{defect} , for different widths (w) and diameters (ρ).

3) Schematic representation of different skyrmionium dynamics states

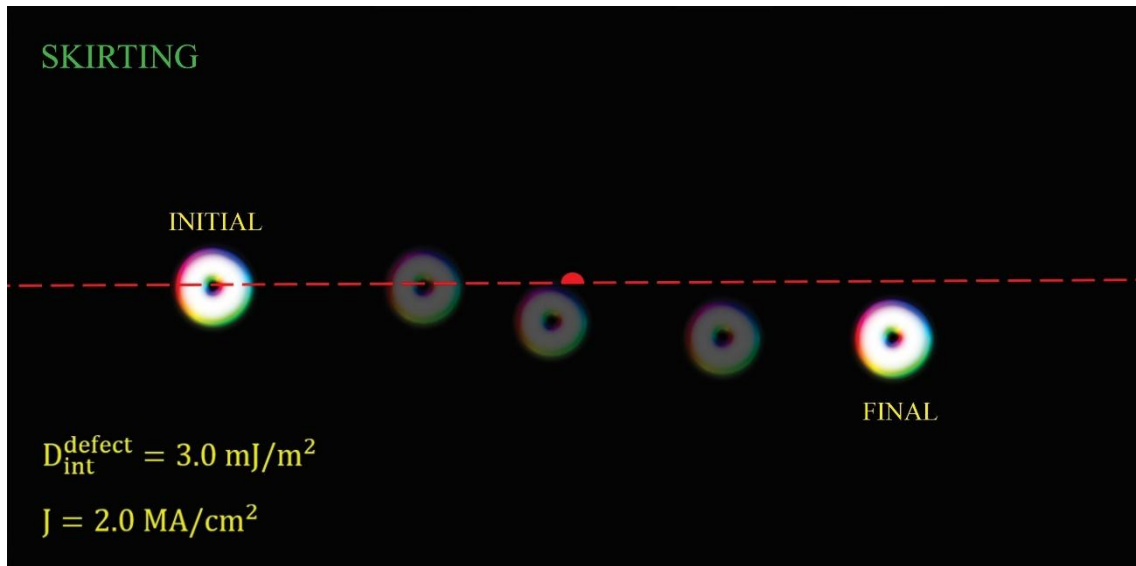


Fig. S13. Representation of the skirting state in which the skyrmionium avoids the magnetic defect to continue its movement along the racetrack.

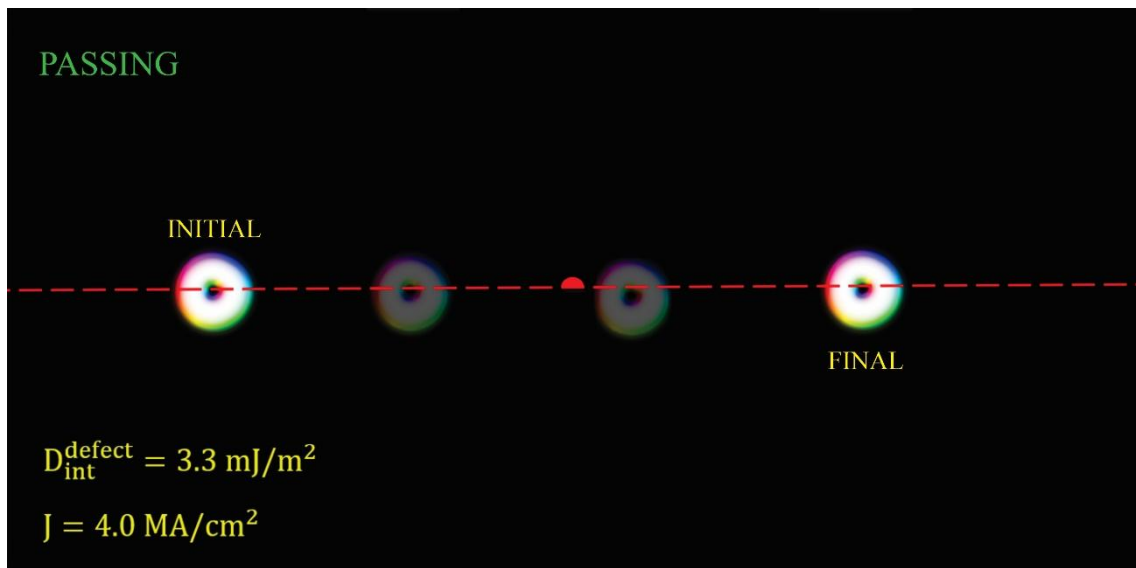


Fig. S14. Representation of the passing state in which the skyrmionium manages to cross the magnetic defect to continue its path along the racetrack.

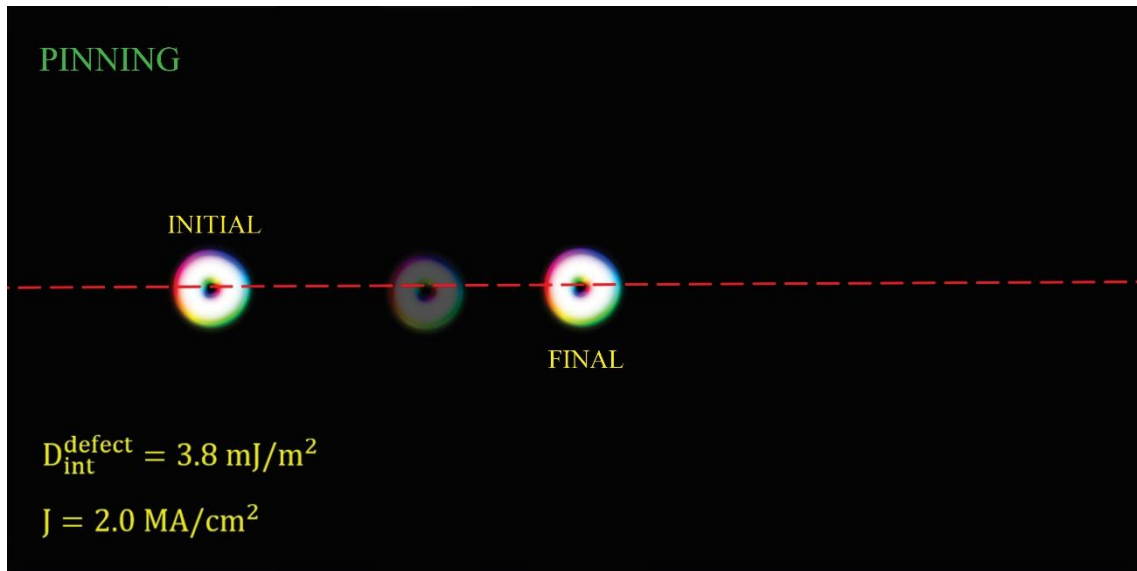


Fig S15: Representation of the pinning state in which the skyrmionium is trapped inside the magnetic defect.

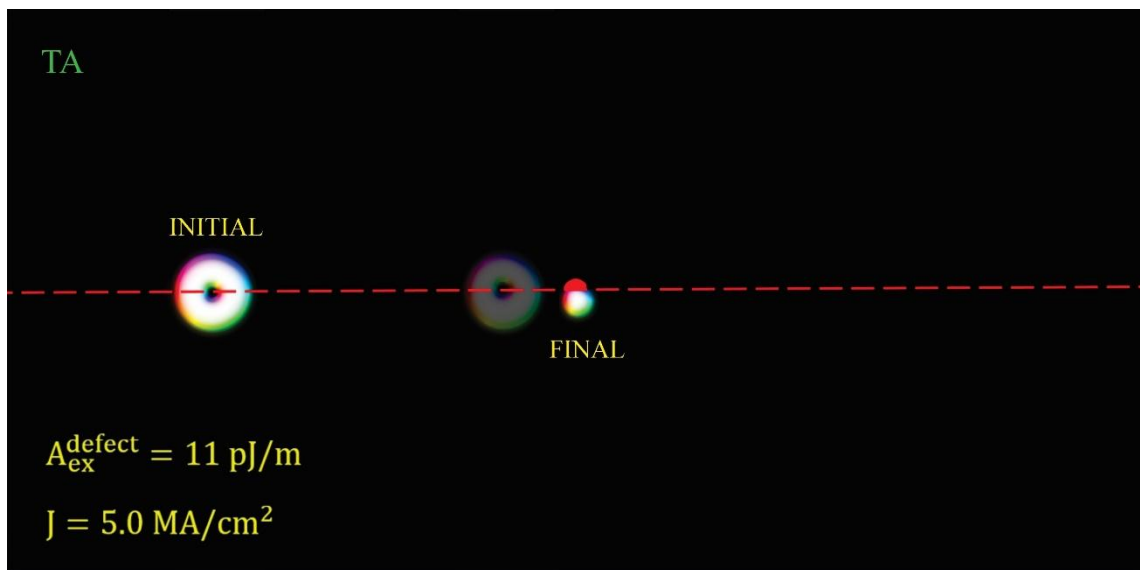


Fig. S16. Representation of the passing state in which a skyrmionium collapses into the defect, transforming into a skyrmion and becoming trapped within the defect.

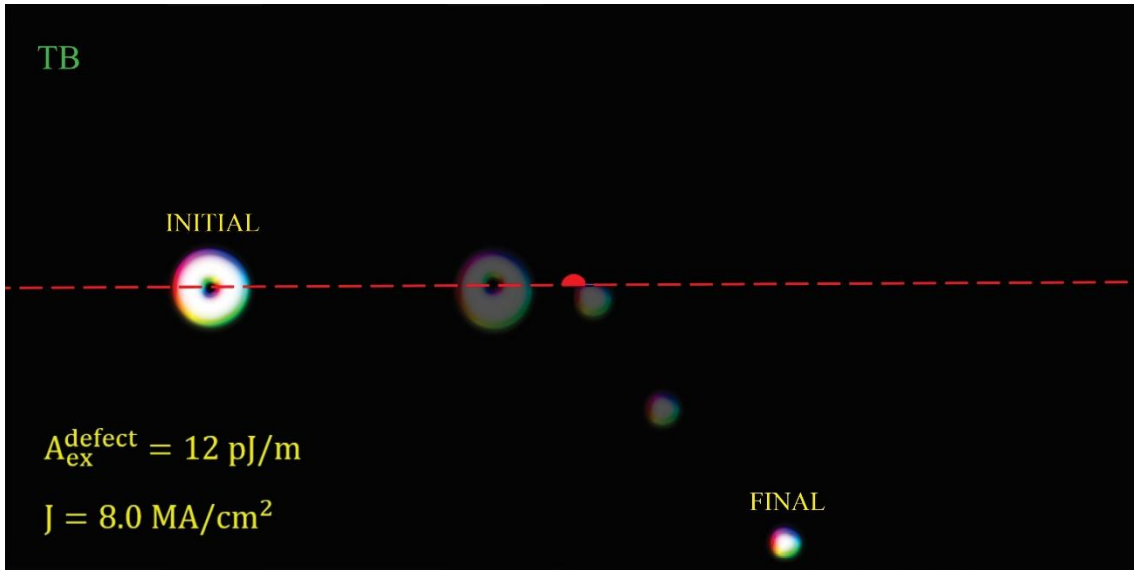


Fig. S17: Schematic representation of a skyrmionium collapsing into a defect, transforming to a skyrmion, and changing path from its original trajectory.

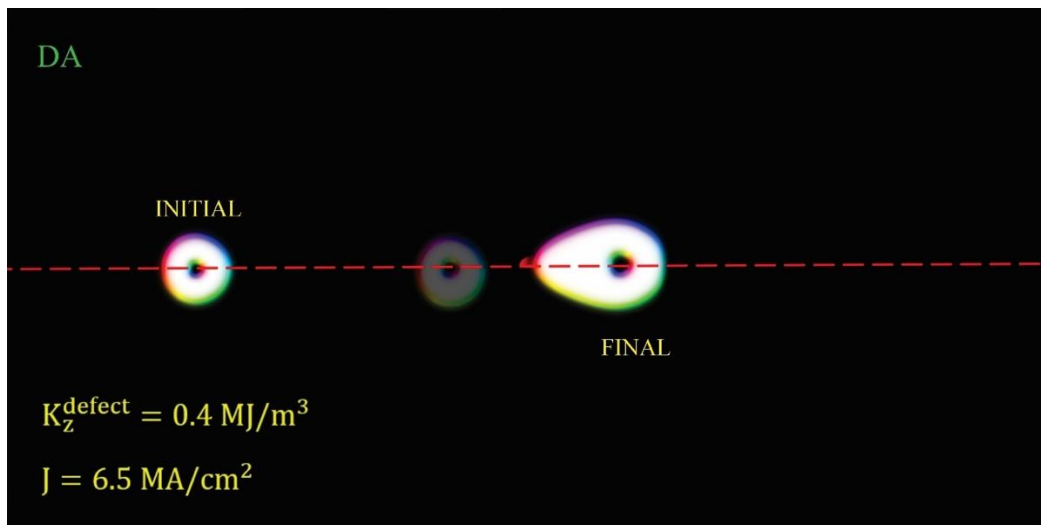


Fig. S18. A schematic representation shows a skyrmionium trapped by a defect. However, due to the current's effect, it deforms and increases in size along the racetrack.



Fig. S19 Schematic representation of the passing state; the skyrmionium stops before colliding with the defect.

4) Skyrmion–Magnetic Defect Interaction Energy

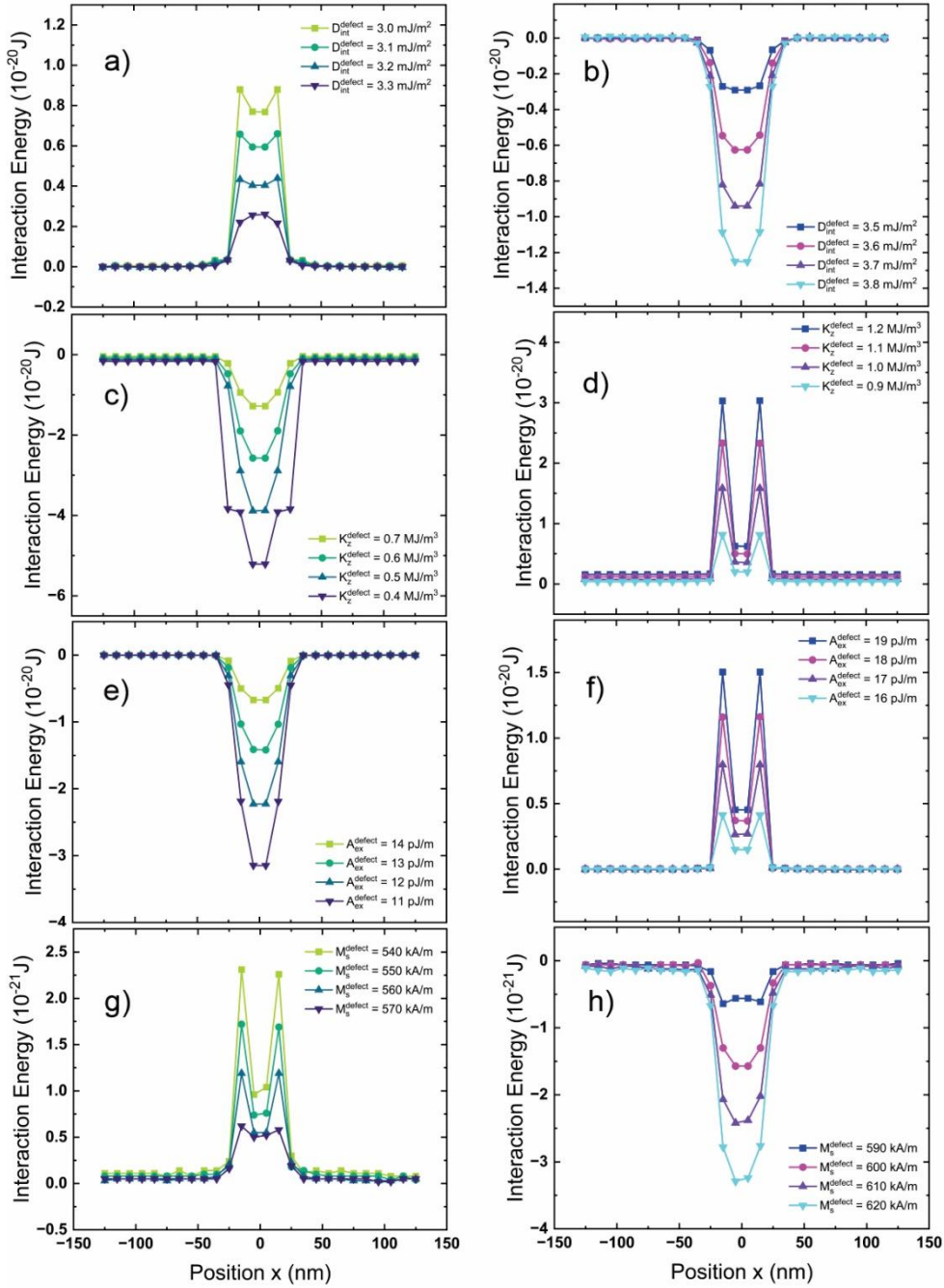


Fig. S19. Interaction energy between the skyrmion and the defect ($\rho = 20 \text{ nm}$) obtained by micromagnetic simulation using eq. (1) considering different defect parameters with a width of $W = 512 \text{ nm}$

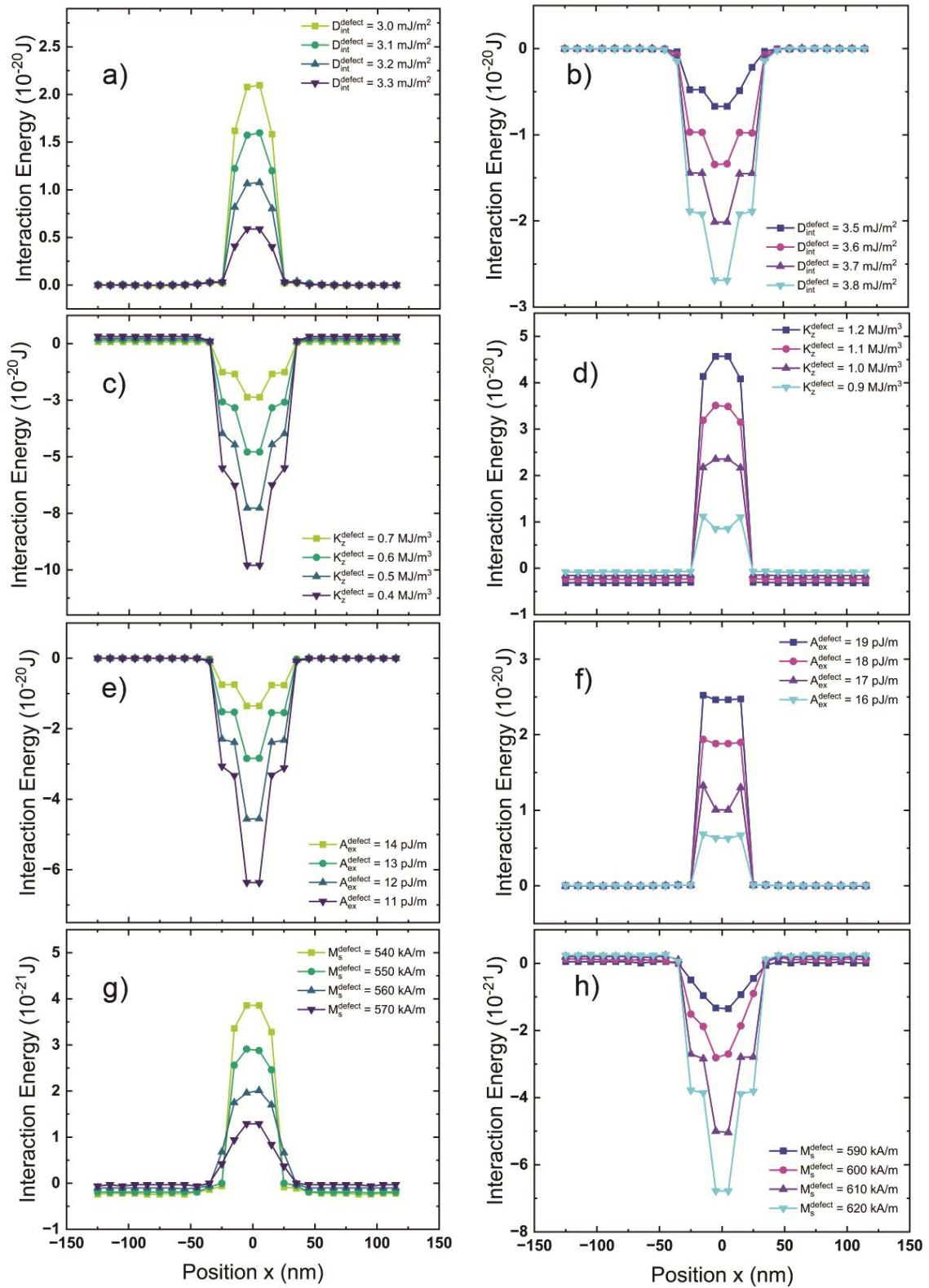


Fig. S20. Interaction energy between the skyrmion and the defect ($\rho = 30$ nm) obtained by micromagnetic simulation using eq. (1) considering different defect parameters with a width of $W = 512$ nm

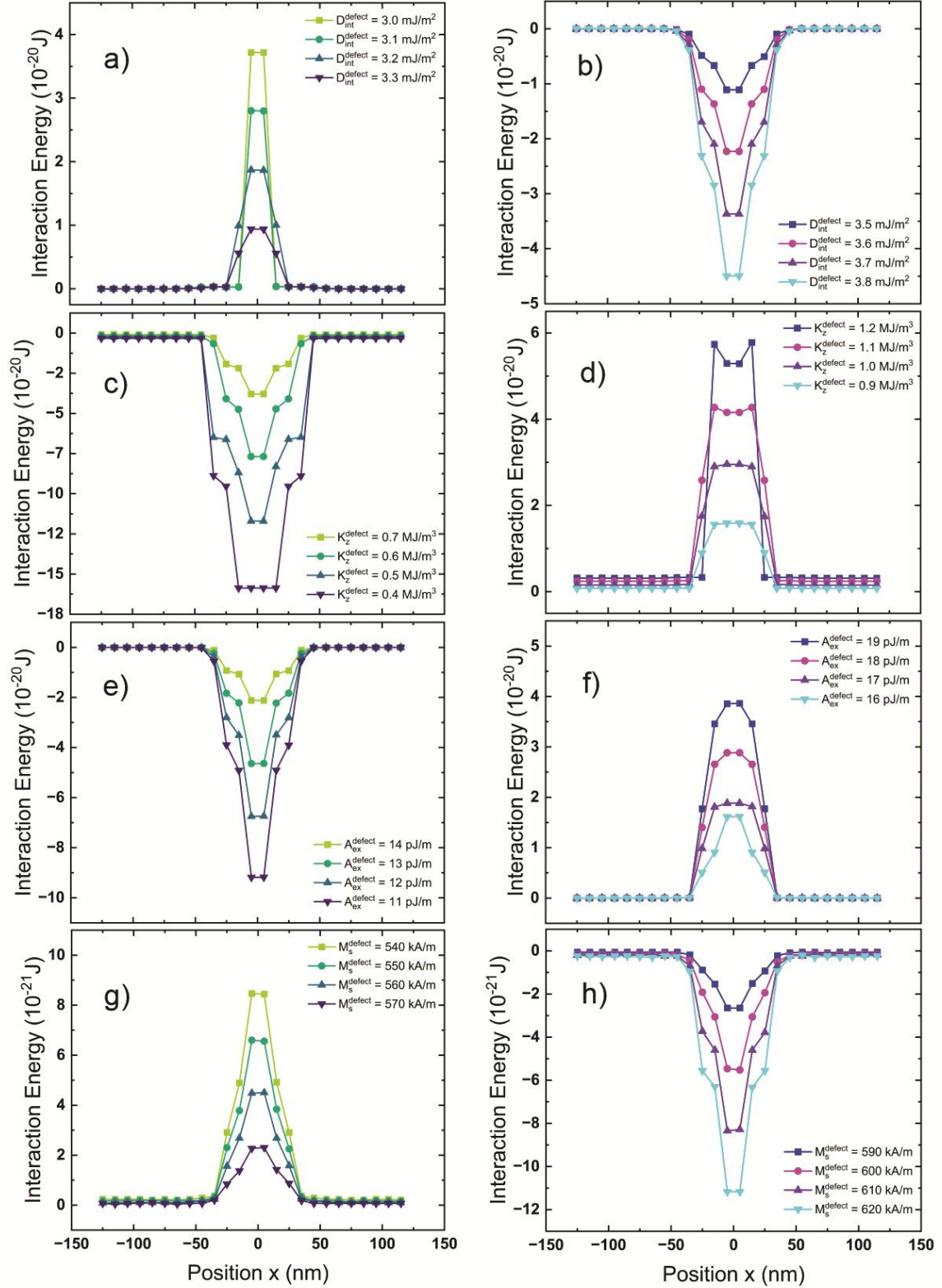


Fig. S21. Interaction energy between the skyrmion and the defect ($\rho = 40$ nm) obtained by micromagnetic simulation using eq. (1) considering different defect parameters with a width of $W = 512$ nm

5) References

- [1] A. Vansteenkiste, J. Leliaert, M. Dvornik, M. Helsen, F. Garcia-Sanchez, and B. Van Waeyenberge, “The design and verification of MuMax3,” *AIP Adv.* 4, 107133 (2014).